Letter

Impact of fluctuating initial conditions on bottomonium suppression in 5.02 TeV heavy-ion collisions

Huda Alalawi,[1] Jacob Boyd,[1] Chun Shen,[2,3] and Michael Strickland[1]
[1]*Department of Physics, Kent State University, Kent, Ohio 44242, USA*
[2]*Department of Physics and Astronomy, Wayne State University, Detroit, Michigan 48201, USA*
[3]*RIKEN BNL Research Center, Brookhaven National Laboratory, Upton, New York 11973, USA*

(Received 18 November 2022; accepted 6 March 2023; published 17 March 2023)

We compute bottomonium suppression and elliptic flow within the potential nonrelativistic quantum chromodynamics effective field theory using an open quantum systems approach. For the hydrodynamical background, we use $2+1$D MUSIC second-order viscous hydrodynamics with IP-glasma initial conditions and evolve bottom/antibottom quantum wave packets in real time in these backgrounds. We find that the impact of fluctuating initial conditions is small when compared to results obtained using smooth initial conditions. Including the effect of fluctuating initial conditions, we find that the $\Upsilon(1S)$ integrated elliptic flow is $v_2[1S] = 0.005 \pm 0.002 \pm 0.001$, with the first and second variations corresponding to statistical and systematic theoretical uncertainties, respectively.

DOI: 10.1103/PhysRevC.107.L031901

I. INTRODUCTION

The strong suppression of bottomonium production in heavy-ion collisions relative to their production in proton-proton collisions is a smoking gun for the creation of a hot quark-gluon plasma (QGP) in relativistic heavy-ion collisions [1–10]. In the seminal work of Matsui and Satz [11], such suppression was proposed as a signal of the formation of a color-ionized QGP which resulted from Debye screening of chromoelectric fields in a QGP. In recent years it was shown that, in addition to Debye screening of the real part of the potential, there also exists an imaginary contribution to the potential, which results in large in-medium widths for heavy quarkonium bound states [12–19].

Including the imaginary part of the potential in calculations results in bottomonium states having widths on the order of 10–100 MeV in the QGP, which must be taken into account in phenomenological descriptions. Resummed perturbative and effective field theory calculations of the imaginary part of the heavy-quark potential have been confirmed by lattice quantum chromodynamics (QCD) measurements of the imaginary part of the potential [20–26] and complex potential models have been quite successful phenomenologically [27–35]. These studies have provided strong evidence that a self-consistent quantum mechanical description of heavy quarkonium in the QGP is possible.

The formalism used in this work is based on recent advances in our understanding of nonrelativistic effective field theory (EFT) and real-time evolution in open quantum systems (OQS) [36]. Such descriptions can model both screening effects and in-medium dynamical transitions between different color and angular momentum states. Recently, there has been a great deal of work on the application of OQS methods to heavy-quarkonium suppression [37–53]. Herein, we will apply OQS methods within the framework of the potential nonrelativistic QCD (pNRQCD) EFT [54–56], which can be obtained systematically from nonrelativistic QCD [57,58]. The pNRQCD EFT relies on there being a large separation between the energy scales in the problem, which is guaranteed for systems where the velocity of the heavy quark relative to the center of mass is small, i.e., $v \ll 1$. Such EFTs can also be used to study quarkonium at finite temperature [13,15,17–19]. Here, we will assume the following scale hierarchy: $1/r \gg m_D \sim \pi T \gg E$, where r is the typical size of the state, m_D is the Debye screening mass, T is the local QGP temperature, and E is the binding energy of the state.

In Refs. [41–43] the authors derived a Lindblad equation [59,60] for the heavy quarkonium reduced density matrix using the scale hierarchy above. Recently, it has become possible to solve the Lindblad equation obtained numerically [61]. The resulting code, called QTRAJ, relies on a Monte Carlo quantum trajectories algorithm [32–34,62]. For this purpose, the Lindblad solver was coupled to a $3+1$D viscous hydrodynamics code that used smooth (optical) Glauber initial conditions [63,64]. The authors found that this provided a quite reasonable description of existing experimental data for both the nuclear modification factor, R_{AA}, and elliptic flow, v_2. It was also found in Refs. [32–34] that, to a very good approximation, one can compute the survival probability of quarkonium states by ignoring the off-diagonal jump terms that change the quantum numbers of the state, evolving instead with a self-consistently determined complex Hamiltonian for singlet states.

Herein, we make the first study of the effect fluctuations in the initial geometry have on bottomonium suppression and flow using an OQS framework that includes the real-time evolution of the bottomonium wave function in a complex potential. Also for the first time, for the hydrodynamic background of the quantum evolution, we make use of the MUSIC hydrodynamics package with fluctuating IP-glasma initial conditions. The IP-glasma initial conditions incorporate gluon saturation effects in the initial state [65–67] and allow one to faithfully describe the early-time dynamics of the QGP.

Previous studies of the impact of fluctuations on bottomonium suppression were reported in Refs. [68,69], where comparisons between smooth Glauber and Monte Carlo Glauber (MC-Glauber) initial conditions using a temperature-dependent disassociation rate. Recently, in Ref. [70] the authors made use of MC-Glauber initial conditions and the SONIC hydrodynamics code [71] to make predictions for bottomonium production in pp, pA, and AA collisions. In Ref. [70], R_{AA} was computed in the adiabatic approximation, by incorporating a temperature- and p_T-dependent width [72]. Finally, in Ref. [50] the authors considered fluctuating initial conditions in the context of a OQS-derived transport model. Herein, we will focus on AA collisions, but go beyond the adiabatic approximation and transport models by solving for the real-time quantum mechanical evolution along each sampled bottomonium trajectory. This is particularly important at early times and in the presence of fluctuating initial conditions, since the temperature can depend strongly on proper time.

II. METHODOLOGY

To compute bottomonium survival probabilities, we evolve the bottom-antibottom wave function forward in time using a time-dependent complex effective Hamiltonian that is accurate to next-to-leading order (NLO) in the binding energy over temperature [34,38]. It can be expressed in terms of two parameters, κ and γ, that can be obtained from a time-ordered correlator of chromoelectric fields and set the magnitude of the decay widths and mass shifts of the states, respectively.

When expressed as operators acting on the reduced wave function, $u = rR(r)$, the NLO singlet effective Hamiltonian $H_s^{\rm eff}$ is given by [34]

$$\mathrm{Re}\big[H_s^{\rm eff}\big] = \frac{\nabla^2}{M} - \frac{C_F\,\alpha_{\rm s}}{r} + \frac{\hat{\gamma}T^3}{2}r^2 + \frac{\hat{\kappa}T^2}{4M}\{r, p_r\}, \quad (1)$$

$$\mathrm{Im}\big[H_s^{\rm eff}\big] = -\frac{\hat{\kappa}T^3}{2}\left[\left(r - \frac{N_c\alpha_{\rm s}}{8T}\right)^2 - \frac{3}{2MT} + \frac{\nabla^2}{(2MT)^2} + \frac{1}{2MT}\left(\frac{N_c\alpha_{\rm s}}{4T}\right)\frac{1}{r}\right], \quad (2)$$

where M is the heavy quark mass, T is the local temperature, N_c is the number of colors, $C_F = (N_c^2-1)/2N_c$, α_s is the strong coupling, $\hat{\kappa} = \kappa/T^3$, $\hat{\gamma} = \gamma/T^3$, $p_r = -i\partial_r$, and $\nabla^2 = -\partial_r^2 + l(l+1)/r^2$. The values of $\hat{\kappa}$ and $\hat{\gamma}$ were taken from direct and indirect lattice measurements and the uncertainty bands and central values used herein are the same as in Ref. [34]. We take the heavy quark mass to be $M = M_{1S} = 4.73$ GeV and the strong coupling is set at the scale of the inverse Bohr radius to be $\alpha_s(1/a_0) = 0.468$ [34].

We evolved all bottom/antibottom quantum wave packets with this effective Hamiltonian and ignored the effects of off-diagonal quantum jumps. This has been shown to be a very good approximation in QCD by prior works [32–34]. To solve for the real-time evolution of each quantum wave packet, we used the Crank-Nicolson method on a one-dimensional lattice with $\texttt{NUM} = 2048$ points, $\texttt{L} = 40\,\mathrm{GeV}^{-1}$, and $\texttt{dt} = 0.001\,\mathrm{GeV}^{-1}$ [73]. The input for the quantum evolution was the temperature experienced by the wave packet as it traverses the QGP.

For the background QGP evolution, we considered 5.02 TeV Pb-Pb collisions modeled by the MUSIC viscous hydrodynamics package [74–76], which includes the effects of both shear and bulk viscosity [77,78]. For the hydrodynamic initial conditions, we use IP-glasma fluctuating initial conditions, which incorporate the effects of the dense gluonic environment generated in nucleus-nucleus collisions [65–67]. We considered $2+1$D boost-invariant evolution using MUSIC with a box size of $L = 30$ fm and 512 grid points in the x and y directions. The equation of state used was based on the HotQCD lattice result [79,80]. The shear viscosity to entropy density ratio was $\eta/s = 0.12$ and we made use of a temperature-dependent bulk viscosity [81]. With these parameters, the MUSIC hydrodynamics code is able to well describe, e.g., charged particle multiplicities, identified hadron spectra, and identified hadron anisotropic flow coefficients [81].

Ensembles of hydrodynamic events with IP-glasma fluctuating initial conditions were sorted into 11 centrality bins. [82] In each centrality bin, we initialized the bottomonium evolution by sampling the initial production points from the fluctuating initial binary collision profile, which automatically includes correlations with the local hot spots generated in each event. The initial transverse momentum was sampled from a $1/E_T^4$ spectrum and the azimuthal angle of the momentum direction was sampled uniformly in $[0, 2\pi)$. We assumed that the quantum wave packets traveled along eikonal trajectories with fixed transverse momentum and azimuthal angle, and sampled the temperature along each trajectory generated. For all results presented herein, we sampled 200 000 wave packet trajectories.

To initialize the real-time quantum evolution along each sampled trajectory, we assumed that at $\tau = 0$ fm the wave function was a smeared δ function and that the system was in the singlet state, with either $l = 0$ or $l = 1$ as the angular momentum quantum number. We took the initial reduced wave function u to be $u_\ell(t_0) \propto r^{l+1}e^{-r^2/(ca_0)^2}$, with $c = 0.2$ [61,83]. We evolved the initial wave function using the vacuum potential from $\tau = 0$ fm to $\tau_{\rm med} = 0.6$ fm and when the temperature along the trajectory considered dropped below $T_F = 190$ MeV. This lower temperature cutoff was fixed by analyzing the convergence of the singlet width when going from LO to NLO in E/T [34].

At the end of each wave packet's evolution, we computed the survival probability of each of the vacuum eigenstates by projecting each final time-evolved wave function with vacuum bottomonium eigenstates. We then accounted for late time

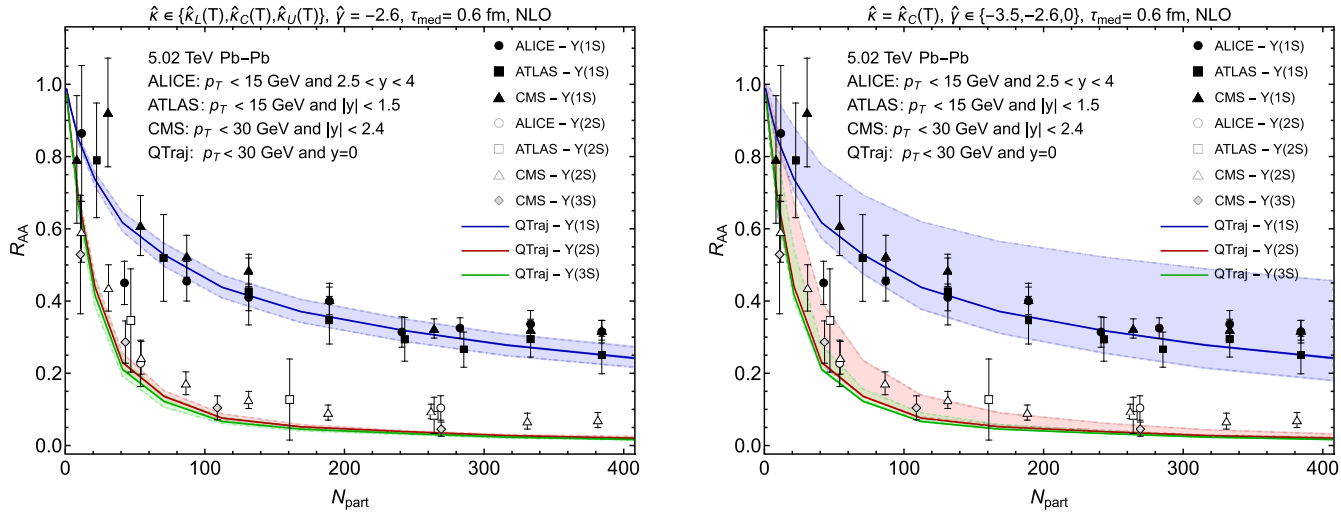

FIG. 1. The nuclear suppression factor R_{AA} for the $\Upsilon(1S)$, $\Upsilon(2S)$, and $\Upsilon(3S)$ states as a function of $N_{\rm part}$ obtained with IP-glasma initial conditions. The left panel shows variation of $\hat{\kappa}$ and the right panel shows variation of $\hat{\gamma}$. The experimental measurements shown are from the ALICE [1], ATLAS [2], and CMS [3,10] collaborations.

feed down of the excited states following Ref. [32]. For this purpose, a feed down matrix F that relates the experimentally observed and direct production cross sections, $\vec{\sigma}_{\rm exp} = F\vec{\sigma}_{\rm direct}$, was used. In our analysis, the states considered were $\vec{\sigma} = \{\Upsilon(1S),\ \Upsilon(2S),\ \chi_{b0}(1P),\ \chi_{b1}(1P),\ \chi_{b2}(1P),\ \Upsilon(3S),\ \chi_{b0}(2P),\ \chi_{b1}(2P),\ \chi_{b2}(2P)\}$. The entries of F are $F_{ij} = B_{j\to i}$ for $i < j$, $F_{ij} = 1$ for $i = j$, and $F_{ij} = 0$ for $i > j$, where $B_{j\to i}$ is the branching fraction of state j into state i taken from Ref. [84]. We used the same branching fractions as prior papers [32–34].

We compute the nuclear modification factor R^i_{AA} for bottomonium state i using

$$R^i_{AA}(c, p_T, \phi) = \left\langle\left\langle \frac{(F \cdot S(c, p_T, \phi) \cdot \vec{\sigma}_{\rm direct})^i}{\vec{\sigma}^{\,i}_{\rm exp}} \right\rangle\right\rangle, \qquad (3)$$

where i labels the bottomonium state being considered, $S(c, p_T, \phi)$ is the survival probability computed from the quantum mechanical evolution, c labels the event centrality class, p_T is the transverse momentum of the bottomonium state, and ϕ its azimuthal angle. The angle brackets indicate a double average over (1) all physical trajectories of bottomonium states and (2) the hydrodynamic initial conditions. For the integrated experimental cross sections we used $\vec{\sigma}_{\rm exp} = \{57.6, 19, 3.72, 13.69, 16.1, 6.8, 3.27, 12.0, 14.15\}$ nb [3,85]. For details concerning the procedure used to obtain these cross sections, see Sec. 6.4 of Ref. [32]. To obtain v_2, we computed $\langle\langle\cos(2(\phi - \Psi_2))\rangle\rangle_{i,c,p_T}$, where the average is over all bottomonium states of type i produced in the corresponding centrality and transverse momentum bins and Ψ_2 is second-order event plane angle determined by final-state charged hadrons. Note that Ψ_2 changes from event to event depending on the initial condition.

III. RESULTS

In Fig. 1 we present our results for R_{AA} as a function of the number of participants, $N_{\rm part}$, compared to experimental data. In both panels our statistical errors are on the order of the line width. In the right panel, the line in the center of the bands has $\hat{\gamma} = -2.6$ which is the value that provided the best agreement with the data in Ref. [34]. We find, similar to Refs. [32–34], that the variation of R_{AA} with $\hat{\kappa}$ is much smaller than the variation with $\hat{\gamma}$. This provides motivation for more constraining extractions of $\hat{\gamma}$ from lattice QCD studies.

Results for the case of optical Glauber initial conditions using the same setup can be found in Refs. [32,33] where slightly lower statistics were used [86]. A comparison of the results shown in Fig. 1 with those prior results demonstrates that the inclusion of fluctuating initial conditions results in quite small changes in R_{AA}, with the differences being smaller than the systematic theoretical uncertainties. From this figure, we see that the $R_{AA}[\Upsilon(1S)]$ is well reproduced, however, the amount of suppression for the $\Upsilon(2S)$ is over predicted for $N_{\rm part} \gtrsim 80$. This could be due to the fact that the pNRQCD approach used works best for the ground state which has a smaller size than the excited states. It could also be due to the fact that in this work we did not include the effect of off-diagonal quantum jumps in the dynamical evolution, which matter more for the excited states than the ground state [32].

In Fig. 2 we present our results for R_{AA} as a function of the transverse momentum, p_T. As in Fig. 1, we see that the variation with $\hat{\gamma}$ is much larger than with $\hat{\kappa}$. Compared to the results obtained with optical Glauber initial conditions (see the figures in Refs. [33,34]), once again we find very little difference between smooth and fluctuating initial conditions. For both types of initial conditions we find that the suppression of the $\Upsilon(1S)$ and $\Upsilon(3S)$ predicted by the NLO OQS+pNRQCD approach agrees well with experimental observations, however, there is some tension between the predictions and the

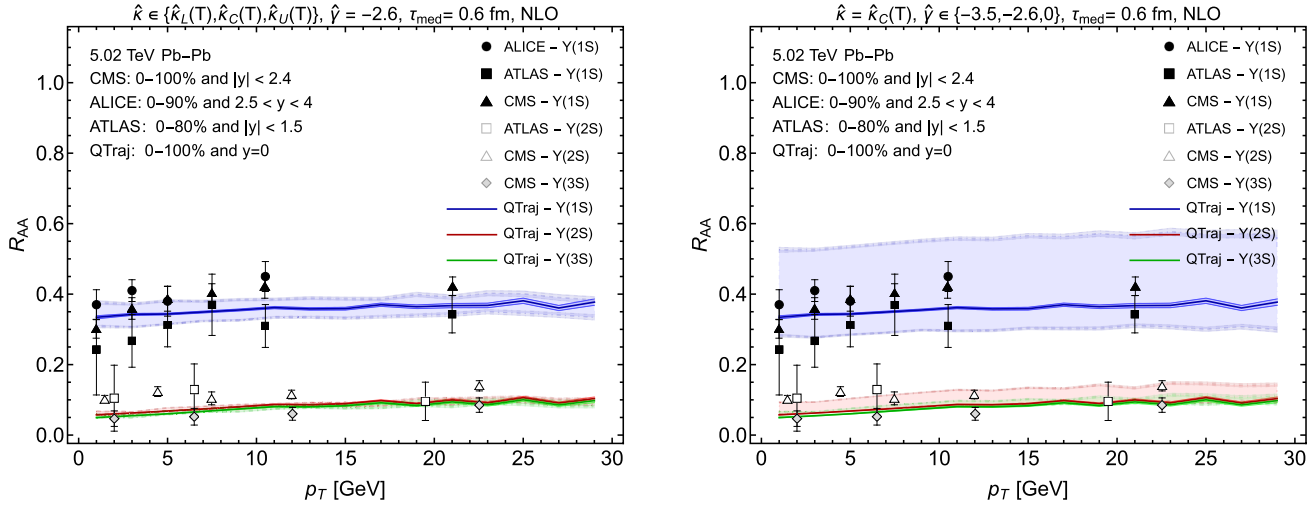

FIG. 2. The nuclear suppression factor R_{AA} for the $\Upsilon(1S)$, $\Upsilon(2S)$, and $\Upsilon(3S)$ states as a function of p_T obtained with IP-glasma initial conditions. The bands and experimental data sources are the same as Fig. 1.

observed $\Upsilon(2S)$ suppression. Despite this, we find that the framework predicts that there is a very weak dependence on p_T which is consistent with experimental observations. This should be contrasted with the p_T dependence of J/ψ suppression observed at CERN Large Hadron Collider (LHC) energies, where the experimental data indicate a strong increase in R_{AA} at low p_T consistent with recombination of liberated charm/anticharm quarks [87,88].

In Fig. 3 we present our predictions for the anisotropic flow coefficient v_2 as a function of centrality in the left panel and transverse momentum in the right panel. We compare our predictions with experimental data from the ALICE and CMS collaborations [5,6]. As the left panel of Fig. 3 demonstrates, the NLO OQS+pNRQCD framework predicts a rather flat dependence on centrality, with the maximum v_2 being on the order of 1%. In the right portion of the left panel, we present the results integrated over centrality in the 10–90 % range. Note, importantly, that the scale of the right portion of the left panel is different from the left portion of this panel. The size of the error bars reflects the statistical uncertainty associated with the double average over initial conditions and physical trajectories and the light shaded regions correspond to the uncertainty associated with the variation of $\hat{\kappa}$ and $\hat{\gamma}$, respectively.

Considering both variations, we find that when integrated in the 10–90 % centrality interval and $p_T < 50$ GeV, $v_2[1S] = 0.005 \pm 0.002 \pm 0.001$, with the first number corresponding to the statistical uncertainty and the second the systematic uncertainty associated with the variation of both $\hat{\kappa}$ and $\hat{\gamma}$. Within statistical uncertainties, this is consistent with the results reported in Refs. [30,33,89], where optical Glauber initial conditions were used. There are hints of a slight decrease in the integrated $v_2[1S]$, however, the decrease is within our statistical uncertainty. Finally, turning to the right panel of Fig. 3 we see that the dependence of $v_2[1S]$ on transverse momentum is rather flat, however, at low momentum there

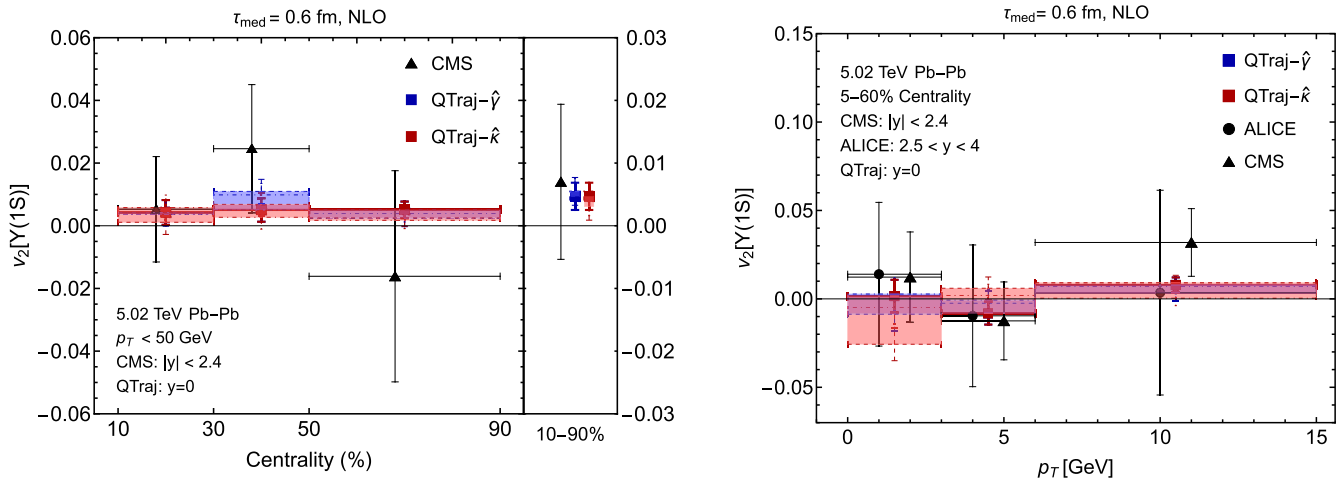

FIG. 3. The anisotropic flow coefficient v_2 as a function of centrality (left) and transverse momentum (right) obtained with IP-glasma initial conditions. We show the $\hat{\gamma}$ variation in blue and the $\hat{\kappa}$ variation in red and compare to experimental data from the ALICE and CMS collaborations [5,6].

is a stronger dependence on $\hat{\kappa}$, which could help to further constrain this parameter in the future.

IV. CONCLUSIONS

In this paper we presented the first results concerning the impact of fluctuating hydrodynamic initial conditions on bottomonium production within a dynamical OQS approach. The complex Hamiltonian used for the quantum evolution is accurate to NLO in the binding energy over temperature, having been recently obtained in Ref. [34]. Due to the computational demand of averaging over both bottomonium trajectories and fluctuating initial conditions, herein we have ignored the effect of dynamical quantum jumps, which have been shown to be small in Refs. [32,33]. In a forthcoming longer paper, we will present predictions for the elliptic flow of $2S$ and $3S$ excited states, along with predictions for higher-order anisotropic flow coefficients such as v_3 and v_4 of all states.

Looking to the future, it will be important to determine the effect of off-diagonal quantum jumps. Given sufficient computational resources, this can be accomplished using the quantum trajectories code. It would also be interesting to see if full three-dimensional fluctuating initial conditions have any impact on the rapidity dependence of these observables. Finally, one outstanding theoretical uncertainty of our work is the effect of the center of mass velocity of the quarkonium state being different than the local flow velocity of the QGP. This effect should be more pronounced when including fluctuating initial conditions, since the flow velocity is more nonuniform, however, it has not yet been included in phenomenological models, even with smooth initial conditions.

ACKNOWLEDGMENTS

H.A. was supported by Umm Al-Qura University Grant No. 22UQU4331035DSR02. J.B. and M.S. were supported by DOE Award No. DE-SC0013470 and C.S. by DOE Award No. DE-SC0021969.

[1] S. Acharya *et al.* (ALICE Collaboration), Phys. Lett. B **822**, 136579 (2021).
[2] Songkyo Lee (CMS Collaboration), Observation of the Υ(3S) meson and sequential suppression of Υ states in PbPb collisions at $\sqrt{s_{\rm NN}} = 5.02$ TeV, CERN, Geneva, https://cds.cern.ch/record/2805926 (2022).
[3] A. M. Sirunyan *et al.* (CMS Collaboration), Phys. Lett. B **790**, 270 (2019).
[4] A. M. Sirunyan *et al.* (CMS Collaboration), Phys. Rev. Lett. **120**, 142301 (2018).
[5] A. M. Sirunyan *et al.* (CMS Collaboration), Phys. Lett. B **819**, 136385 (2021).
[6] S. Acharya *et al.* (ALICE Collaboration), Phys. Rev. Lett. **123**, 192301 (2019).
[7] L. Adamczyk *et al.* (STAR Collaboration), Phys. Lett. B **735**, 127 (2014); **743**, 537 (2015).
[8] A. Adare *et al.* (PHENIX Collaboration), Phys. Rev. C **91**, 024913 (2015).
[9] L. Adamczyk *et al.* (STAR Collaboration), Phys. Rev. C **94**, 064904 (2016).
[10] Soohwan Lee (CMS Collaboration), Observation of the $\Upsilon(3S)$ meson and sequential suppression of states in PbPb collisions at $\sqrt{s_{NN}} = 5.02$ TeV, Quark Matter 2022, Krakow, Poland, https://indico.cern.ch/event/895086/contributions/4716202/ (2022).
[11] T. Matsui and H. Satz, Phys. Lett. B **178**, 416 (1986).
[12] M. Laine, O. Philipsen, P. Romatschke, and M. Tassler, J. High Energy Phys. 03 (2007) 054.
[13] N. Brambilla, J. Ghiglieri, A. Vairo, and P. Petreczky, Phys. Rev. D **78**, 014017 (2008).
[14] A. Beraudo, J.-P. Blaizot, and C. Ratti, Nucl. Phys. A **806**, 312 (2008).
[15] M. A. Escobedo and J. Soto, Phys. Rev. A **78**, 032520 (2008).
[16] A. Dumitru, Y. Guo, and M. Strickland, Phys. Rev. D **79**, 114003 (2009).
[17] N. Brambilla, M. A. Escobedo, J. Ghiglieri, J. Soto, and A. Vairo, J. High Energy Phys. 09 (2010) 038.
[18] N. Brambilla, M. A. Escobedo, J. Ghiglieri, and A. Vairo, J. High Energy Phys. 12 (2011) 116.
[19] N. Brambilla, M. A. Escobedo, J. Ghiglieri, and A. Vairo, J. High Energy Phys. 05 (2013) 130.
[20] A. Rothkopf, T. Hatsuda, and S. Sasaki, Phys. Rev. Lett. **108**, 162001 (2012).
[21] A. Rothkopf, Phys. Rep. **858**, 1 (2020).
[22] P. Petreczky, A. Rothkopf, and J. Weber, Nucl. Phys. A **982**, 735 (2019).
[23] D. Bala and S. Datta, Phys. Rev. D **101**, 034507 (2020).
[24] M. Laine, O. Philipsen, and M. Tassler, J. High Energy Phys. 09 (2007) 066.
[25] A. Lehmann and A. Rothkopf, J. High Energy Phys. 07 (2021) 067.
[26] K. Boguslavski, B. S. Kasmaei, and M. Strickland, J. High Energy Phys. 10 (2021) 083.
[27] M. Strickland, Phys. Rev. Lett. **107**, 132301 (2011).
[28] M. Strickland and D. Bazow, Nucl. Phys. A **879**, 25 (2012).
[29] B. Krouppa, R. Ryblewski, and M. Strickland, Phys. Rev. C **92**, 061901(R) (2015).
[30] A. Islam and M. Strickland, J. High Energy Phys. 03 (2020) 235.
[31] A. Islam and M. Strickland, Phys. Lett. B **811**, 135949 (2020).
[32] N. Brambilla, M. A. Escobedo, M. Strickland, A. Vairo, P. Vander Griend, and J. H. Weber, J. High Energy Phys. 05 (2021) 136.
[33] N. Brambilla, M. A. Escobedo, M. Strickland, A. Vairo, P. Vander Griend, and J. H. Weber, Phys. Rev. D **104**, 094049 (2021).
[34] N. Brambilla, M. A. Escobedo, A. Islam, M. Strickland, A. Tiwari, A. Vairo, and P. Vander Griend, J. High Energy Phys. 08 (2022) 303.
[35] L. Wen and B. Chen, arXiv:2208.10050 [nucl-th].
[36] H. Breuer and F. Petruccione, *The Theory of Open Quantum Systems* (Oxford University Press, Oxford, 2002).
[37] Y. Akamatsu and A. Rothkopf, Phys. Rev. D **85**, 105011 (2012).
[38] Y. Akamatsu, Prog. Part. Nucl. Phys. **123**, 103932 (2022).

[39] Y. Akamatsu, Phys. Rev. D **91**, 056002 (2015).
[40] T. Miura, Y. Akamatsu, M. Asakawa, and A. Rothkopf, Phys. Rev. D **101**, 034011 (2020).
[41] N. Brambilla, M. A. Escobedo, J. Soto, and A. Vairo, Phys. Rev. D **96**, 034021 (2017).
[42] N. Brambilla, M. A. Escobedo, J. Soto, and A. Vairo, Phys. Rev. D **97**, 074009 (2018).
[43] N. Brambilla, M. A. Escobedo, A. Vairo, and P. Vander Griend, Phys. Rev. D **100**, 054025 (2019).
[44] R. Sharma and A. Tiwari, Phys. Rev. D **101**, 074004 (2020).
[45] J.-P. Blaizot, D. De Boni, P. Faccioli, and G. Garberoglio, Nucl. Phys. A **946**, 49 (2016).
[46] J.-P. Blaizot and M. A. Escobedo, J. High Energy Phys. 06 (2018) 034.
[47] J.-P. Blaizot and M. A. Escobedo, Phys. Rev. D **98**, 074007 (2018).
[48] J.-P. Blaizot and M. A. Escobedo, Phys. Rev. D **104**, 054034 (2021).
[49] X. Yao and T. Mehen, Phys. Rev. D **99**, 096028 (2019).
[50] X. Yao, W. Ke, Y. Xu, S. A. Bass, and B. Müller, J. High Energy Phys. 01 (2021) 046.
[51] X. Yao and T. Mehen, J. High Energy Phys. 02 (2021) 062.
[52] X. Yao, Int. J. Mod. Phys. A **36**, 2130010 (2021).
[53] R. Katz and P. B. Gossiaux, Ann. Phys. (NY) **368**, 267 (2016).
[54] A. Pineda and J. Soto, Nucl. Phys. B Proc. Suppl. **64**, 428 (1998).
[55] N. Brambilla, A. Pineda, J. Soto, and A. Vairo, Nucl. Phys. B **566**, 275 (2000).
[56] N. Brambilla, A. Pineda, J. Soto, and A. Vairo, Rev. Mod. Phys. **77**, 1423 (2005).
[57] W. Caswell and G. Lepage, Phys. Lett. B **167**, 437 (1986).
[58] G. T. Bodwin, E. Braaten, and G. P. Lepage, Phys. Rev. D **51**, 1125 (1995); **55**, 5853(E) (1997).
[59] V. Gorini, A. Kossakowski, and E. Sudarshan, J. Math. Phys. **17**, 821 (1976).
[60] G. Lindblad, Commun. Math. Phys. **48**, 119 (1976).
[61] H. B. Omar, M. A. Escobedo, A. Islam, M. Strickland, S. Thapa, P. Vander Griend, and J. H. Weber, Comput. Phys. Commun. **273**, 108266 (2022).
[62] J. Dalibard, Y. Castin, and K. Molmer, Phys. Rev. Lett. **68**, 580 (1992).
[63] M. Alqahtani and M. Strickland, Eur. Phys. J. C **81**, 1022 (2021).
[64] H. Alalawi, M. Alqahtani, and M. Strickland, Symmetry **14**, 329 (2022).
[65] J. Bartels, K. J. Golec-Biernat, and H. Kowalski, Phys. Rev. D **66**, 014001 (2002).
[66] H. Kowalski and D. Teaney, Phys. Rev. D **68**, 114005 (2003).
[67] B. Schenke, P. Tribedy, and R. Venugopalan, Phys. Rev. Lett. **108**, 252301 (2012).
[68] T. Song, K. C. Han, and C. M. Ko, arXiv:1112.0613 [nucl-th].
[69] T. Song, K. C. Han, and C. M. Ko, J. Phys.: Conf. Ser. **420**, 012023 (2013).
[70] J. Kim, J. Seo, B. Hong, J. Hong, E.-J. Kim, Y. Kim, M. Kweon, S. H. Lee, S. Lim, and J. Park, arXiv:2209.12303 [nucl-th].
[71] SONIC, https://bitbucket.org/mhabich/sonic/src/master/ (2017).
[72] J. Hong and S. H. Lee, Phys. Lett. B **801**, 135147 (2020).
[73] For a systematic study of the lattice spacing and step size dependence, we refer the reader to Ref. [61].
[74] B. Schenke, S. Jeon, and C. Gale, Phys. Rev. C **82**, 014903 (2010).
[75] B. Schenke, S. Jeon, and C. Gale, Phys. Rev. C **85**, 024901 (2012).
[76] MUSIC v3.0, https://github.com/MUSIC-fluid/MUSIC (2022).
[77] S. Ryu, J. F. Paquet, C. Shen, G. S. Denicol, B. Schenke, S. Jeon, and C. Gale, Phys. Rev. Lett. **115**, 132301 (2015).
[78] J.-F. Paquet, C. Shen, G. S. Denicol, M. Luzum, B. Schenke, S. Jeon, and C. Gale, Phys. Rev. C **93**, 044906 (2016).
[79] A. Bazavov *et al.*, Phys. Rev. D **80**, 014504 (2009).
[80] A. Bazavov *et al.* (HotQCD Collaboration), Phys. Rev. D **90**, 094503 (2014).
[81] B. Schenke, C. Shen, and P. Tribedy, Phys. Rev. C **102**, 044905 (2020).
[82] The evolution files used are publicly available on Google Drive, https://drive.google.com/drive/folders/1rEF7Cfe2DMHmZmlUyGvMW4RjM5BijqMt?usp=share_link.
[83] Observables do not depend significantly on c below this value [32–34,61].
[84] P. A. Zyla *et al.* (Particle Data Group), PTEP **2020**, 083C01 (2020).
[85] R. Aaij *et al.* (LHCb Collaboration), Eur. Phys. J. C **74**, 3092 (2014).
[86] We have explicitly verified that, when the number of physical trajectories are the same, the results obtained using optical Glauber initial conditions are nearly identical to the results obtained herein.
[87] J. Adam *et al.* (ALICE Collaboration), Phys. Lett. B **766**, 212 (2017).
[88] A. M. Sirunyan *et al.* (CMS Collaboration), Eur. Phys. J. C **78**, 509 (2018).
[89] P. P. Bhaduri, M. Alqahtani, N. Borghini, A. Jaiswal, and M. Strickland, Eur. Phys. J. C **81**, 585 (2021).